





Article

Dynamic Remote Sensing Prediction for Wheat Fusarium Head Blight by Combining Host and Habitat Conditions

Yingxin Xiao ^{1,2}, Yingying Dong ^{1,2,*} , Wenjiang Huang ^{1,2,3}, Linyi Liu ¹ , Huiqin Ma ¹ ,
Huichun Ye ^{1,3}  and Kun Wang ¹

¹ Key Laboratory of Digital Earth Science, Aerospace Information Research Institute, Chinese Academy of Sciences, Beijing 100094, China; 842850478x@gmail.com (Y.X.); huangwj@aircas.ac.cn (W.H.); liuly35@radi.ac.cn (L.L.); mahq0712@nuist.edu.cn (H.M.); yehc@radi.ac.cn (H.Y.); wangkun@radi.ac.cn (K.W.)

² University of Chinese Academy of Sciences, Beijing 100190, China

³ Key Laboratory for Earth Observation of Hainan Province, Sanya 572029, China

* Correspondence: dongyy@aircas.ac.cn; Tel.: +86-10-82178178

Received: 10 August 2020; Accepted: 17 September 2020; Published: 18 September 2020



Abstract: Remote sensing technology provides a feasible option for early prediction for wheat Fusarium head blight (FHB). This study presents a methodology for the dynamic prediction of this classic meteorological crop disease. Host and habitat conditions were comprehensively considered as inputs of the FHB prediction model, and the advantages, accuracy, and generalization ability of the model were evaluated. Firstly, multi-source satellite images were used to predict growth stages and to obtain remote sensing features, then weather features around the predicted stages were extracted. Then, with changes in the inputting features, the severity of FHB was dynamically predicted on February 18, March 6, April 23, and May 9, 2017. Compared to the results obtained by the Logistic model, the prediction with the Relevance Vector Machine performed better, with the overall accuracy on these four dates as 0.71, 0.78, 0.85, and 0.93, and with the area under the receiver operating characteristic curve as 0.66, 0.67, 0.72, and 0.75. Additionally, compared with the prediction with only one factor, the integration of multiple factors was more accurate. The results showed that when the date of the remote sensing features was closer to the heading or flowering stage, the prediction was more accurate, especially in severe areas. Though the habitat conditions were suitable for FHB, the infection can be inhibited when the host's growth meets certain requirements.

Keywords: wheat; fusarium head blight; dynamic prediction; remote sensing; multiple factors

1. Introduction

Fusarium head blight (FHB), also known as scab, is an economically devastating disease of wheat caused by *Fusarium graminearum* (*Gibberella zeae*) [1]. In the past decade, China has witnessed the aggravation of FHB, both in scope and severity, causing significant economic losses in wheat [2,3]. Wheat FHB frequently occurs in the middle and lower reaches of the Yangtze River and has gradually spread to the northwest, covering more than 10 major agricultural areas. What is worse, infected wheat will produce mycotoxins, notably deoxynivalenol (DON) and zearalenone (ZEA), which may lead to acute poisoning symptoms and physical damage [4–6]. Given the frequent occurrences and rapid development of FHB epidemics, the prediction for wheat FHB in a precise time and space scale is of great significance, and provides reliable and timely management advice for wheat producers and valuable time for food operators or processors to properly detect and manage damaged grain.

There are two main methods to predict wheat FHB. The first is mainly based on a statistical model, utilizing the relationship between meteorological conditions and the occurrence of FHB. The second concentrates on the change in spectrum when crops are infected with diseases, describing crop stress by spectral features extracted from various sensors. Because the appropriate temperature, rainfall, and relative humidity around wheat are the main factors for the reproduction of the pathogen [7], a method to judge the severity of disease in the field by combining weather forecast data with microclimate measurements has been developed [8–10]. Besides this, the change in crop structure and pigment in the process of the highly specific disease will result in a change in reflectance. Therefore, as an effective method in object detection over large areas, satellite-based remote sensing technology, has been widely used in plant disease monitoring or prediction, and diverse vegetation indices (VIs) have been brought up. For instance, Yudarwati et al. analyzed multi-temporal satellite images to put forward a vegetation index suitable for monitoring rice bacterial blight. The results showed that three indexes, Normalized Difference Green/Red Index (NGRDI), Normalized Pigment Chlorophyll Index (NPCI), and Plant Senescence Reflectance Index (PSRI), had the highest correlation with the occurrence of bacterial blight, with an R^2 0.44, 0.63, and 0.67, respectively [11]. Such methods take into consideration the habitat or the growth conditions, respectively, during the most susceptible stages of the crop to the disease, which proved to be useful in disease prediction. Although they have been applied in practice and are still under continuous refinement, newer prediction algorithms are proposed. It is crucial to predict disease earlier and more accurately, especially in a more precise time scale.

Taking all these factors into consideration, in current state of the art research, researchers have utilized a disease prediction methodology combining habitat and growth conditions, providing an emerging idea for early disease prediction [12]. For example, Ma et al. used Landsat-8 images to extract VIs and Land Surface Temperature (LST), and spatially interpolated the daily weather data, as inputs of the Relevance Vector Machine to predict wheat powdery mildew. The results showed that the overall accuracy of the model constructed by the combination of multiple data was greater than that of the model based on only one type of factor [13]. The prediction method of crop disease combining multiple factors usually considers four key points. The susceptible growth stages of the crop were mostly based on the records of agrometeorological stations or field investigation to choose the suitable growth stages of the crop as the study time [14,15]. Growth conditions: collecting the remote sensing data during the selected stages. VIs and their important trend components in time-series have been widely used in monitoring plant disease stress [16,17]. Many researchers have inverted crop agronomic parameters to detect the growth of crops and the structure of landscapes [18,19]. Habitat conditions: meteorological data have often often used to calculate the indices in a short time range. In addition, remote sensing data can also be employed in retrieving environmental factors [12,20,21]. The selection of a suitable prediction model: there has been an increasing number of mathematical models applied to crop disease prediction, in which machine learning models are widely used [22–24]. The existing research results show that the comprehensive consideration of multi factors can improve prediction accuracy. Based on this, we further tested the ability of this kind of method for FHB prediction.

We focused on the dynamic prediction of winter wheat FHB. Important factors leading to the occurrence and development of FHB, including the host and habitat conditions, were extracted by multi-source remote sensing and other auxiliary data. High temporal and spatial resolution satellite images were respectively used to predict the key growth stages of wheat and to obtain remote sensing features that reflect growth conditions. Meanwhile, habitat conditions were described by weather features during the predicted stages. Then, we analyzed the performance of the Relevance Vector Machine for FHB prediction and mapped the prediction results of FHB severity. The dynamic prediction was realized through inputting features that change with time. Namely, the remote sensing features will change with the acquiring of satellite-based images on different dates, and the weather features will change with the accuracy of the meteorological forecast data.

2. Materials and Methods

2.1. Study Area and Data

Our study was performed in 2017 for Changfeng and Dingyuan County of Anhui Province ($29^{\circ}41'N$ – $34^{\circ}38'N$, $114^{\circ}54'E$ – $119^{\circ}37'E$) (Figure 1). The area was located in the lower reaches of the Yangtze River where the planting area of winter wheat was about 1698 km^2 , accounting for 35% of the total area, and the major cultivar was “Yangmai 25”, susceptible to FHB. In this area, both the planting system and the degree of mechanization were generally unified. The annual accumulated temperature above 0°C there is about 5200°C – 5500°C , and the annual average rainfall is about 960 mm [25]. Because of the influence of the monsoon, the precipitation in spring and summer contributes the most. With a high planting density; a variety susceptible to FHB; sufficient sources of *Gibberella*; and, most importantly, suitable precipitation and temperature conditions, the occurrence of FHB of winter wheat in this area is relatively serious [26]. According to the records, the frequency of the year of a pandemic in this region is as high as 57.1% [27]. As preparation for our experiment, the wheat cultivated areas were classified by the decision tree model, with vegetation indices and characteristics of the Normalized Difference Vegetation Index (NDVI) curve extracted from time-series Moderate Resolution Imaging Spectroradiometer (MODIS) images as inputs.

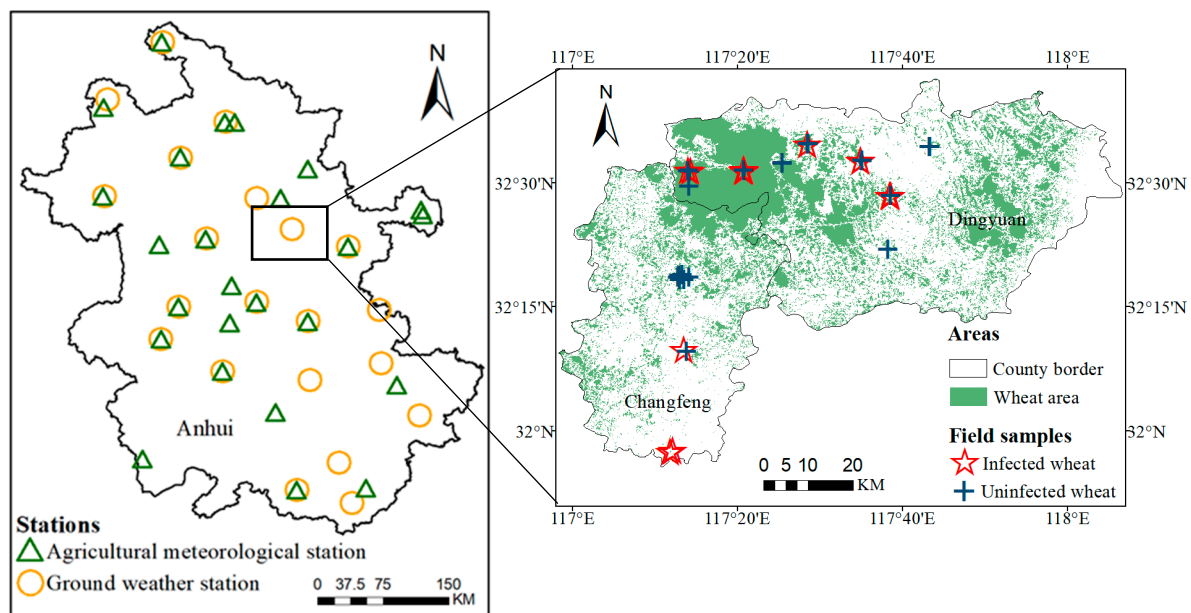


Figure 1. Study area and samplings.

There are three types of data involved in the study: field survey, satellite images, and meteorological data. For the collection of the reference data for FHB prediction, a field investigation was carried out from May 8 to May 9, 2017. The survey included the longitude and latitude of the centers of 45 plots, and the FHB damage percentage to the wheat ears in each plot. The damage conditions of five $1 \times 1 \text{ m}$ ranges in each homogenous plot were investigated, and the average was obtained. We only regarded those plots with a damage percentage equal to zero as uninfected samples, and 45 groups of field samples were obtained (Figure 1). As auxiliary data for selecting remote sensing features, a total of 189 sets of canopy hyperspectral data of infected and uninfected wheat were collected in Anhui Province from April 26 to April 29 and May 8 to May 13. The satellite images contained the level 4 MODIS global Leaf Area Index (LAI) product MCD15A3H from January to June 2014–2017, and the Landsat-8 (L8) surface reflectance product from January to June 2017, in which four L8 images (February 18, March 6, April 23, May 9) of Dingyuan and three images (February 18, April 23, May 9) of Changfeng were obtained. The meteorological data we used included the daily weather data from January to June

2014–2017 and the agrometeorological data in China. Inverse distance weight interpolation (IDW) was employed on the daily weather indices for spatial interpolation with a resolution of 30 m.

2.2. Dynamic Remote Sensing Prediction for Wheat FHB

That situation will be suitable for FHB occurrence when sources of *Fusarium graminearum* in the planting area are sufficient and, more essentially, the host and habitat conditions provide a proper environment for the fungi. Therefore, the host and habitat were synthetically considered. Multi-source remote sensing data, which have been widely used to detect changes in morphology, leaf color, and chlorosis of crops [25,28,29], were utilized to obtain host conditions, including growth stages, with a high time accuracy, and growth conditions in a precise spatial scale. Then, during the most sensitive stages of crops to FHB-causing fungi, we calculated and selected weather indices within narrow periods to reflect habitat conditions. With the optimized remote sensing and weather features as inputs of our prediction model to assess the FHB severity of winter wheat and provide more accurate guidance for fungicide application decisions, the probability of FHB was dynamically predicted through the change in the input features (Figure 2).

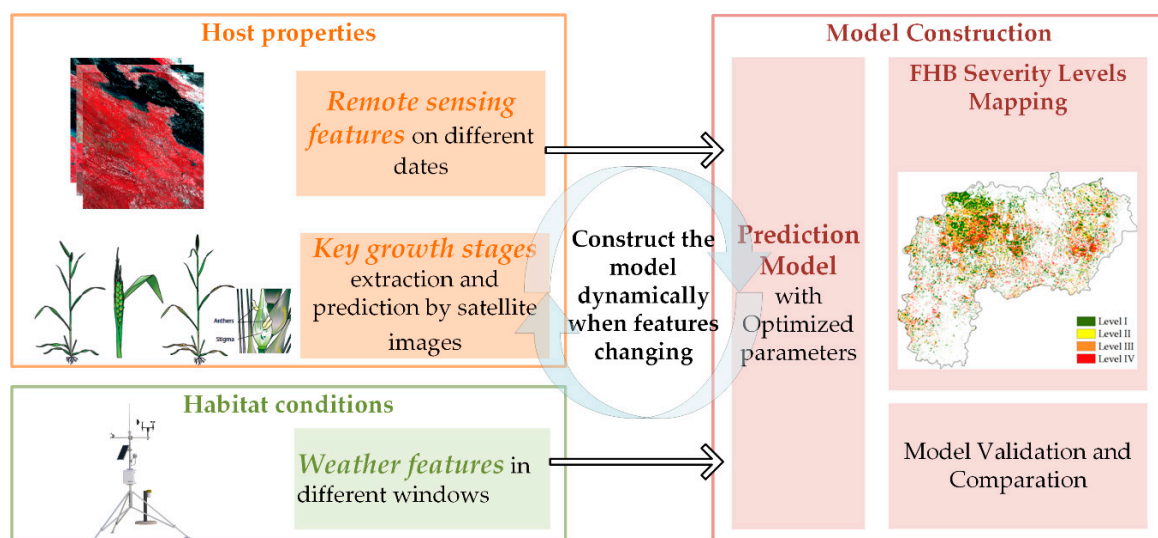


Figure 2. Flow chart of dynamic remote sensing prediction for wheat FHB.

2.2.1. Host and Habitat Conditions Extraction

Comprehensively considering the factors that affect the infection of FHB, we predicted the growth stages, extracted growth, and habitat conditions of crops. The growth stages were predicted through the accumulated temperature and the crop growth curve obtained from time-series satellite-based images. The growth conditions were explained by remote sensing features captured regularly. For the weather features that characterized habitat conditions, the predicted growth stages were identified as their time references.

Firstly, we predicted the heading and flowering dates in the target year based on the average accumulated temperature in former years [30]. That is, the MODIS LAI time-series data were used to extract the green-up and heading dates of winter wheat in past years, and the average accumulated temperature between the two dates was calculated as the threshold for wheat in the target year achieving the heading date from green-up. Similarly, 105 °C was taken as the threshold to predict the flowering date from the heading date [31]. The improved Whittaker smoother [32,33] was chosen to reconstruct the data on time-series MODIS LAI; based on this, the iLAI-Logistic method was utilized to extract the transition date [34,35]. According to the growth characteristics of winter wheat, green-up is the stage of rapid greening for leaves, while heading is the best stage of nutritional and reproductive

growth for the crop, corresponding to the maximum values of the first curvature of cumulative data and that of the reconstructed data, respectively (Figure 3) [35].

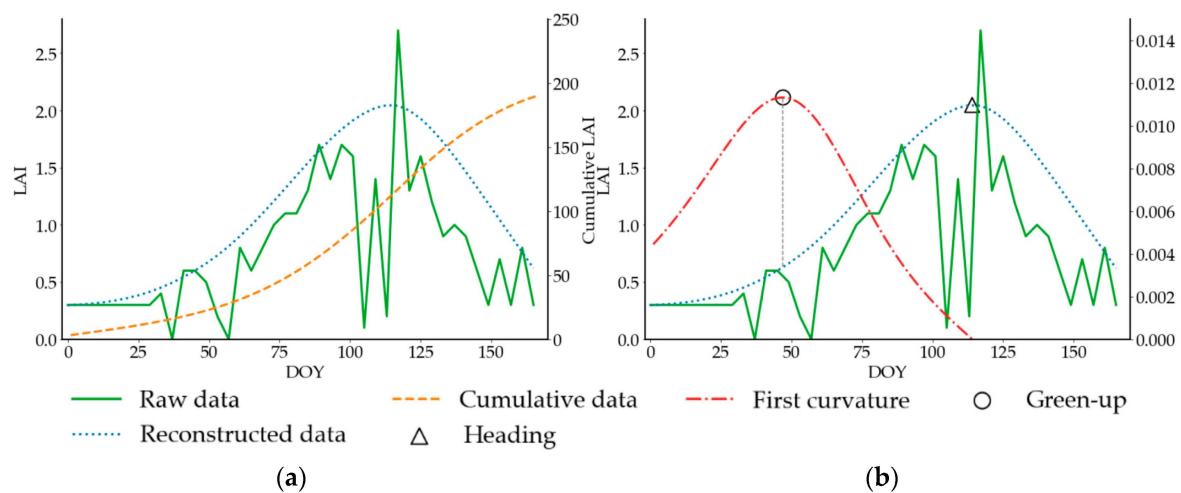


Figure 3. Extraction of Day of Year (DOY) of green-up and heading. (a) The results of Whittaker smoother and the accumulation of reconstructed data. (b) The key points on the first curvature curve and the reconstructed LAI curve.

Wheat FHB usually causes the disease spots on the ear, changing the morphology, leaf color, and chlorosis, which leads to the optics being altered. Therefore, for the selection of remote sensing features to describe crop growth conditions, we mainly considered those who can reflect the nutrition and disease stress of crops. Fourteen spectral indicators, including 4 original bands (Blue, Green, Red, and NIR) and 10 vegetation indexes (VIs) (including Enhanced Vegetation Index (EVI), Normalized Difference Vegetation Index (NDVI), Green Normalized Difference Vegetation Index (GNDVI), Simple Ratio (SR), Triangular Vegetation Index (TVI), Optimized Soil-Adjusted Vegetation Index (OSAVI), Modified Simple Ratio (MSR), Renormalized Difference Vegetation Index (RDVI), Plant Senescence Reflectance Index (PSRI), and Difference Vegetation Index (DVI)) were selected. Among them, for instance, Red and NIR were the bands highly correlated to FHB [25]; PSRI can well reflect the stress of crop canopy [19]. Besides this, NDVI and GNDVI can be used to quantify vegetation greenness or assess photosynthetic activity; TVI describes the radiant energy absorbed by the pigment. On this basis, OSAVI increased the sensitivity to vegetation by using a standard value for the canopy background adjustment, and RDVI increased the sensitivity to biophysical parameters by combining the SR. To improve the accuracy of the prediction model and avoid the problem caused by redundancy between input features, a reselection process was implemented on the 14 indicators. Because spectral indicators are comprehensive in the detection of disease, the Relief algorithm and Pearson correlation were applied. Relief updates the weight of each feature by finding the nearest neighbor samples in two categories repeatedly, indicating the discrimination ability of features to close samples. Meanwhile, the Pearson correlation between two features illustrates the redundancy [36].

As for the weather feature selection, a commonly used method is evaluating the correlation between disease and weather indices in different narrow periods of a certain length (windows) [7], [37–39]. Near the predicted heading to flowering date, we calculated the average temperature (TAVG); average relative humidity (RHAVG); average precipitation (PAVG); average sunshine hours (SSDAVG); days with an RH greater than 60%, 70% and 80% (RH60, RH70, and RH80); days with an RH greater than 60%, 70%, and 80% and a temperature greater than 15 °C and less than 30 °C (RHT60, RHT70, and RHT80); and the number of rainfall days (PDAY) in different narrow time ranges. Since a single weather index has a direct impact on FHB, we focused on the correlation between each index and FHB. Therefore, the Kendall and Pearson correlation coefficients of these indices were calculated.

2.2.2. FHB Prediction with Relevance Vector Machine

As the time approaches the FHB infection period, the conditions of the host and habitat constantly change, which makes it possible for the prediction to be realized dynamically. The remote sensing features used to detect host conditions changed as satellite-based images were regularly obtained. Meanwhile, for weather features, though their time ranges were fixed by the predicted heading and flowering dates, the meteorological data, in practice, should have been forecasted and became more accurate as the time approached. Therefore, the prediction of FHB can be refreshed as long as the satellite-based remote sensing data or the weather forecasting data are updated. Comprehensively combining the remote sensing features on different dates and the weather features around heading to flowering, we put forward the predictions on the corresponding dates.

The field samples with the remote sensing and weather features at different times were respectively split into training and test sets, with the same spatial distribution. Each training set was used to optimize the parameters of the Relevance Vector Machine (RVM) and train the model. It is generally believed that the higher the probability, the closer the sample is to a certain category. Therefore, we concentrated on the probability of classification (PRC), but not simply infected or uninfected. According to the Chinese National Standard GB/T 15796-2011 (rules for the monitoring and prediction of wheat head blight), we split the PRC into four levels. The higher the level, the more likely FHB was to occur: level I ($0 < \text{PRC} \leq 25\%$), level II ($25\% < \text{PRC} \leq 50\%$), level III ($50\% < \text{PRC} \leq 75\%$), level IV ($75\% < \text{PRC} \leq 100\%$). With the selected model, the probability of the FHB of each pixel was obtained, and the FHB severity on the four dates was mapped. Besides, the corresponding test set was utilized to measure the model performance from three aspects. When setting the classification threshold as constant, we considered the total accuracy and combination results of the precision and recall rates. Then, the generalization ability was evaluated.

RVM, proposed by Tipping in 2001, is a sparse probability model with a high generalization ability, suitable for a small number of samples [40,41]. Carried out in the framework of Bayesian, RVM will produce few relevance vectors (RVs) in the training process and obtain the posterior distribution of model parameters through training. In the beginning, we optimized the parameters of RVM. A kernel (K) was used to transform the data into a higher-dimensional space, improving the separability of classification [42,43]. To determine the parameters of the kernel for the better performance of RVM, we applied cross-validation in the training sets [44], and the average overall accuracy (OA) of the corresponding model was calculated. Subsequently, in order to evaluate the performance of the RVM model with the optimal parameters, we measured the ability of the model by test sets. In the beginning, we calculated the overall accuracy to evaluate the accuracy of classification. Then, an index, F1 score, was calculated for a comprehensive consideration of the precision and recall rate [45]. In addition, as class imbalance often occurs in the actual data set, the average receiver operating characteristic curve (ROC) and area under the curve (AUC) were utilized to describe the generalization ability of our model [46]. We randomly split the samples on each date to obtain the ROC curves and calculated the AUC.

Because the most influential factors in the development of FHB occurrence have been considered, including the host the habitat conditions, the prediction was expected to be more accurate and persuasive compared to the system constructed by only one kind of factor. Besides, since RVM can provide a posterior probability estimation in classification, and has a great generalization ability as a result, the probability of FHB was more reliable. Moreover, with the change in the remote sensing features, the development of FHB was explored, and therefore dynamic prediction was realized.

3. Results

3.1. Identification of Host and Habitat Conditions Sensitive to FHB

Host conditions, including growth stages (the heading and flowering dates of crops) and growth conditions (spectral indicators of crop biophysical properties and diseases stress), were respectively

obtained through long time-series MODIS LAI and Landsat-8 images on different dates with a high quality and few clouds covered. Then, the habitat conditions were described by the weather indices around heading to flowering.

The heading and flowering dates of winter wheat in 2017 were predicted with the green-up date regarded as the start, based on the average accumulated temperature between the green-up and heading dates in 2014–2016. Utilizing the Whittaker smoother and iLAI-Logistic method, we extracted the green-up and heading dates of winter wheat in 2014–2016 and the green-up date in 2017. The prediction results of the heading and flowering dates in 2017 based on the average accumulated temperature in the past three years are shown in Figure 4. When comparing the predicted heading dates with the results extracted by MODIS LAI (Figure 5), 57.67% of the pixels had a difference of 0–4 days, 73.7% of them had 0–6 days, and 84.6% had 0–8 days. Namely, the results of the two methods were similar, and the prediction results had a certain reliability. Besides, with the regulations about standards of wheat production in Anhui, about 80–85% of wheat in Anhui Province were planted from October 15 to October 31. Therefore, as for the validation of the extracted green-up and heading dates in 2014–2016, because they highly depended on the seeding time, which was generally similar in these years, we counted the average green-up and heading dates of winter wheat in Anhui Province and in 31 °N–33 °N according to the historical agrometeorological data and took the intersections. It was considered that the extraction results outside the intersection range were the points with larger errors. In general, the proportion of pixels within the intersection range of Dingyuan and Changfeng were 92.5–94.5% and 94.5–97%, respectively—within an acceptable range.

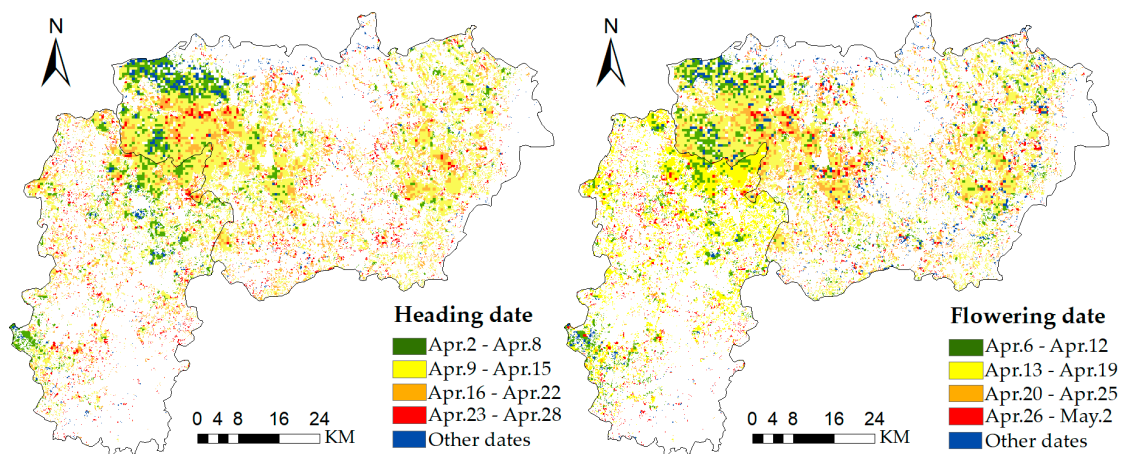


Figure 4. Prediction results of the heading and flowering stages of winter wheat in 2017.

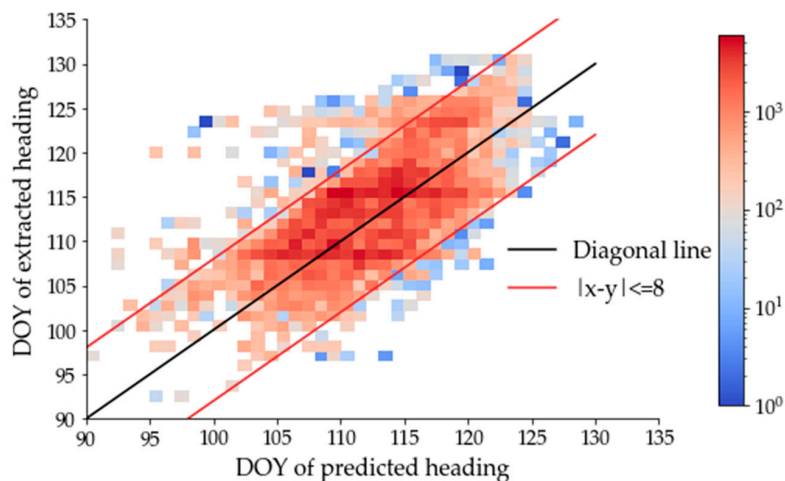


Figure 5. The scatter plot between the DOY of the predicted and extracted heading.

Identifying variables to be used as input features is of great significance to develop a disease prediction system. Two key points need to be taken into consideration: the higher correlation of the feature with FHB or the higher weight of it in FHB classification, and the lower redundancy between these features [36]. For selecting remote sensing features, the hyperspectral data of the wheat canopy, whose spectral resolution was 3 nm in the range of 350–1000 nm, were used to simulate the reflectance of L8 Operational Land Imager (OLI) bands. With the canopies labeled infected or uninfected, we applied the Relief algorithm and Pearson correlation coefficient on the 14 spectral indicators, calculated or extracted from the simulated L8 data. The results of Relief are shown in Figure 6. Subsequently, between the two features with a large Pearson correlation, we had the feature with the higher weight reserved. Finally, four remote sensing features were selected to illustrate the growth of the crops and the development of FHB: PSRI, Green, Red, and NIR. According to this, the four features of the selected L8 images were extracted and synthesized, corresponding to February 18, March 6 (only Dingyuan), April 23, and May 9, respectively.

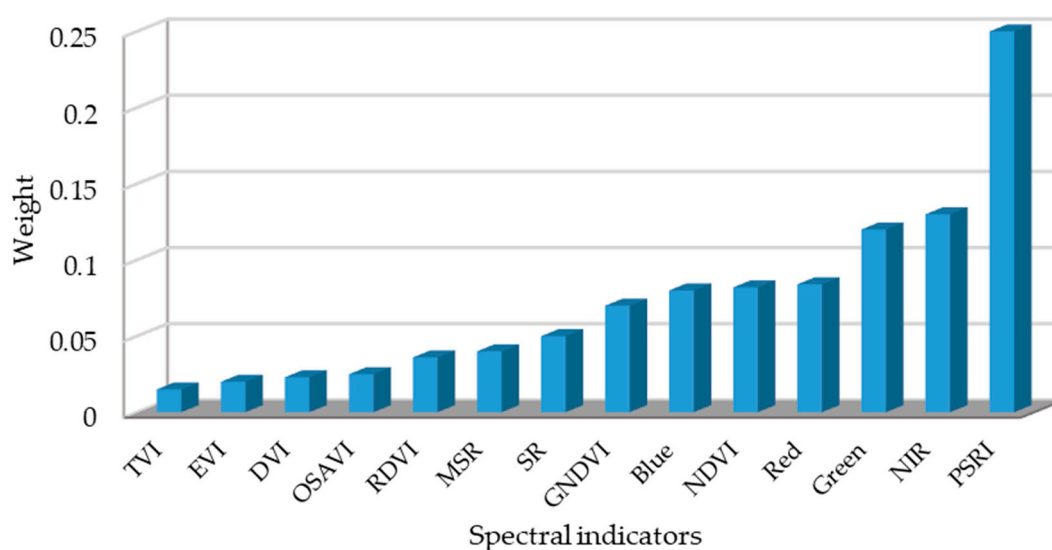


Figure 6. The Relief weight of the remote sensing indicator in FHB recognition.

We obtained 140 weather indices of every field sample with labels (infected or uninfected). Taking 3, 5, 7, 11, and 15 as the length of the time period (window) and regarding the predicted heading date as the last and the middle day of the window, we calculated the pre-heading and heading weather indices, including TAVG, RHAVG, PAVG, SSDAVG, RH60, RH70, RH80, RHT60, RHT70, RHT80, and PDAY. A total of 70 weather indices near the heading date were obtained. Similarly, the pre-flowering and flowering weather indices were calculated in the same way, with the predicted flowering date as a time reference point. Kendall correlation coefficients of the 140 weather indices near the stage of predicted heading to flowering date was calculated by the field samples. We selected the indices whose absolute Kendall correlation was greater than 0.3 and, combined with the results of the Person coefficient between them, we got five weather features which are listed in Table 1.

Table 1. Weather indices selection results based on the Kendall and Pearson correlation coefficients.

Index	Definition	Kendall	<i>p</i> Value
d15RH80	Taking the flowering date as the middle, the duration (days) of 15 days with RH \geq 80%	0.43	0.005
b15RH80	Taking the heading date as the middle, the duration (days) of 15 days with RH \geq 80%	0.42	0.008
d5RHAvg	Taking the flowering date as the middle, the mean value of RH	0.41	0.004
c7TAVG	Mean temperature of 7 days before flowering	0.41	0.009
c7PAVG	The average rainfall of 7 days before flowering	0.39	0.009

3.2. FHB Dynamic Prediction with RVM and Model Validation

To be noticed, the remote sensing features were changed since images were acquired on different days. Whereas, for the weather features, we utilized the measured data from meteorological stations instead of the forecasting data, and hence the weather features of samples were unchanged. That is, each field sample had two kinds of features, in which the remote sensing features changed with the acquisition of satellite-based images, and the weather features were fixed. Combining the PSRI, Green, Red, and NIR of L8 images on different dates and five weather features calculated near the heading or flowering date, we predicted the severity of wheat FHB on February 18, March 6 (only Dingyuan), April 23, and May 9. The cloud cover of the images on the four dates was 0.14%, 11.03%, 1.92%, and 1.62%. On March 6, the cloud was mainly distributed in the north of Changfeng, and hence our prediction on the day was only achieved in Dingyuan. A total of 45 field samples with features on these four dates were respectively split into training and test sets, with a proportion of 7:3. The training sets were used to determine the parameters of RVM, and we constructed prediction models on four dates, calculated the probability of each FHB-infected wheat pixel, and mapped the results. Subsequently, the total accuracy, classification performance, and generation ability of the four-day models were assessed by the corresponding test sets. As a comparison, the Logistic classification model, a common model that was used to get the probability of the classification, was utilized in the same way.

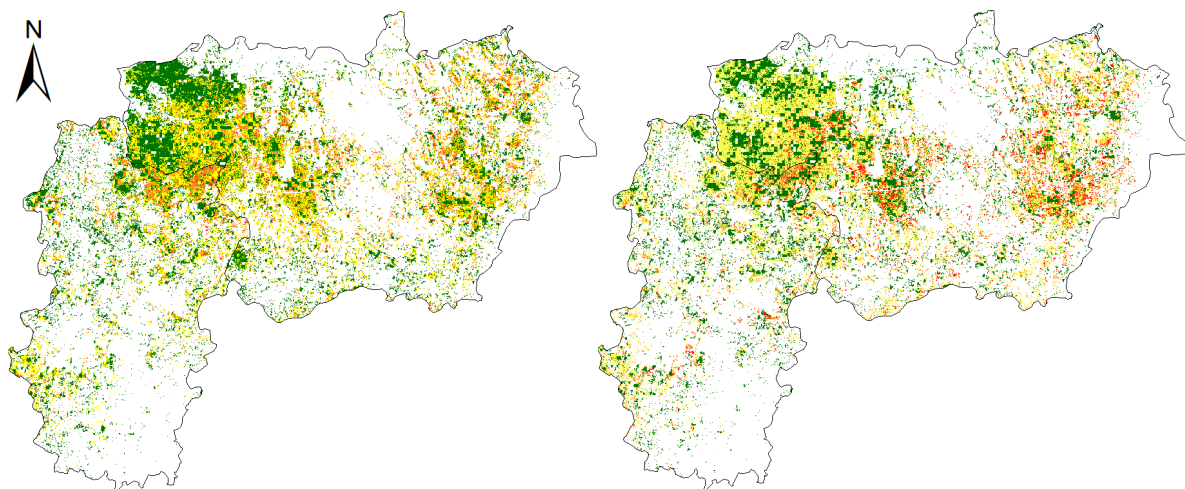
In the beginning, to optimize the parameters of the RVM kernel, we applied a five-fold cross-validation on the training sets on different dates. For the polynomial kernel, γ is the inner product coefficient and d is the dimension. Meanwhile, in the case of the Radial Basis Function (RBF) kernel, γ determines the RBF width. Taking the prediction on April 23 as an example, Table 2 shows the validation results of RVM under different parameters. In our experiment, the performance of RBF was generally better than the polynomial, and the number of RVs was fewer. Because of the fewer parameters and higher accuracy, RBF has been widely used in recent research [22,42,43,47]. In the prediction results based on the combination of weather and remote sensing features on April 23, when γ was equal to 0.01, the accuracy is the highest. Similarly, the parameters of the models utilized on the other three dates (February 18, March 6, and May 9) were decided in the same way.

Table 2. Taking 0.5 as the threshold of probability of classification, the mean of overall accuracy (OA) for five-fold cross-validation, and the number of Relevance Vectors (RVs) for one subset.

Kernel Type	Parameter		Mean of OA	Number of RVs
	γ	d		
RBF	0.0001	-	0.802	11
RBF	0.01	-	0.846	16
RBF	100	-	0.778	11
Polynomial	0.01	3	0.758	23

RVM models with optimized parameters were used to predict the occurrence probability of wheat FHB on four dates in 2017. Meanwhile, the Logistic model was utilized to compare with RVM. The probability was divided into four risk levels, as shown in Figure 7. In general, the situation of wheat FHB in Dingyuan County was more severe in 2017. The risk level of continuous planting area in the northwest and northeast was III or IV, while that in Changfeng County was high in the northeast. When comparing the results of the two models, the distribution of wheat in different severity levels shows little difference, and the regularities were obvious; when the remote sensing features were closer to the stage of heading to flowering, the prediction of the areas with severe disease was more accurate, and these areas showed aggregation in the mapping. In total, over time, the areas of grade I were fewer, the areas of risk grade IV increased, and the grade II and III areas were changing to other grades thus with a small change. Compared with the results of the RVM, the prediction probability of the Logistic model is larger on February 18 and March 6 and smaller on April 23 and May 9 in general areas.

Further, we compared our results with those predicted using only the selected weather and only the remote sensing features on April 23 with RVM (Figure 8). Compared with the prediction with multiple factors, by and large the severity of the results obtained by only using the remote sensing features was less, and when only using the meteorological features it was higher. Except in some areas, the prediction results using only one kind of feature were similar, such as the western part of Dingyuan County, where the probabilities were all smaller than that predicted from the multiple factor combination. The comparison showed that FHB was the result of the comprehensive effects of host and habitat conditions; even if the meteorological conditions were conducive to the occurrence of FHB, the growth of crops would still affect the further development of it.



(a) February 18.

Figure 7. Cont.

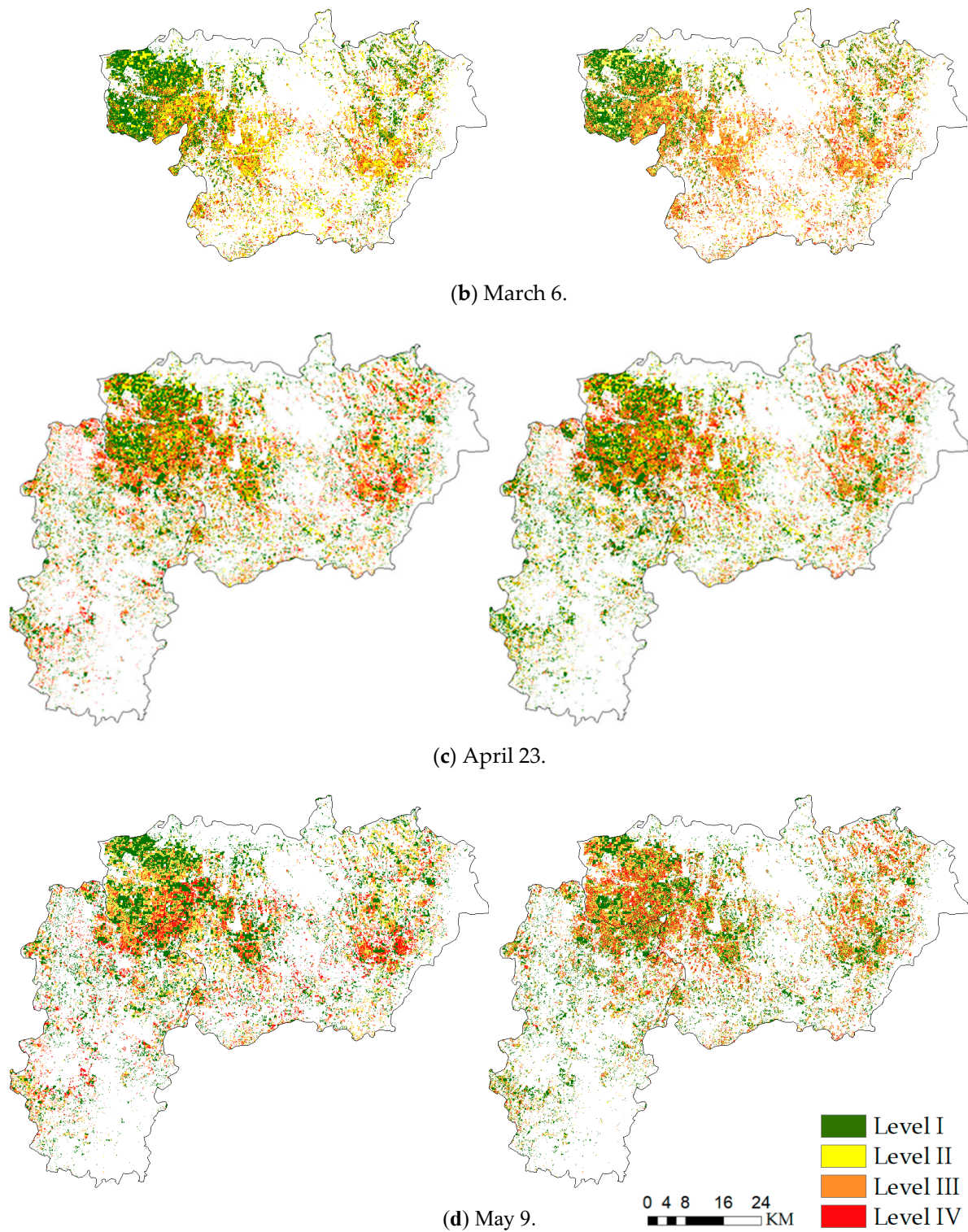


Figure 7. Prediction results of the FHB severity. According to the Chinese National Standard, the severity was divided into four risk levels. (a–d) The results of RVM (left) and Logistic (right), utilizing the remote sensing features in four dates.

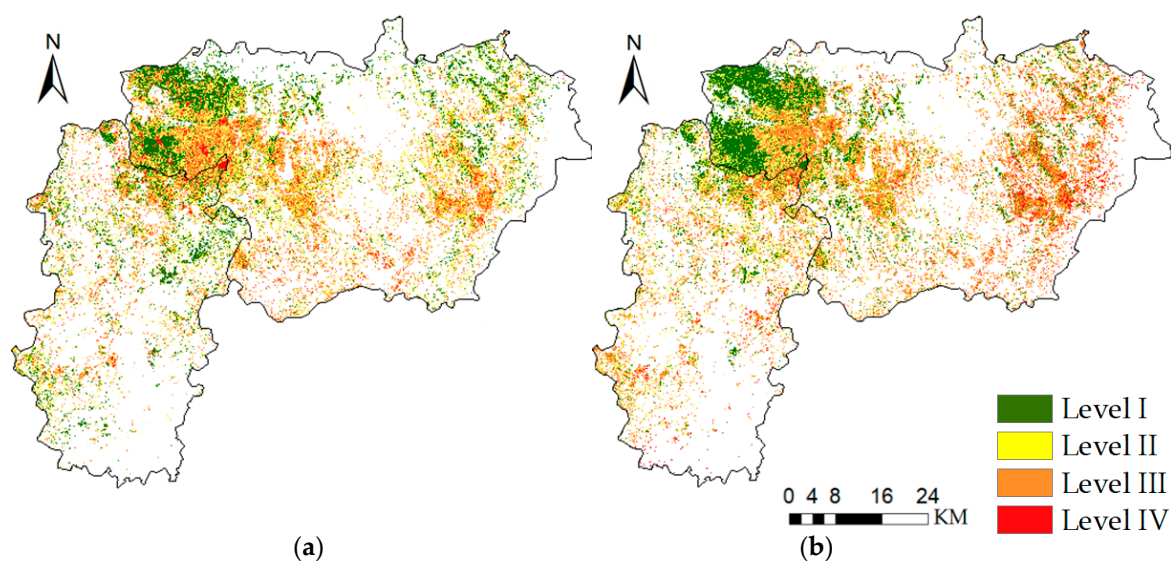


Figure 8. Prediction results utilizing only one factor. (a) The result obtained using the remote sensing features on April 23. (b) By the selected weather features.

To evaluate the advantages of RVM in predicting the wheat FHB, we compared the performance between the RVM and the Logistic model. The value of 0.5 was set as the threshold of probability to calculate the overall accuracy and the F1 score of the two models on different dates (Table 3). In total, the prediction accuracy of RVM was higher than that of the Logistic model. From the results, it is apparent that when the date of remote sensing features was close to the stage of heading to flowering, the prediction accuracy of the two models was higher, which showed that the remote sensing features can reflect the development of FHB to a certain extent.

Table 3. Overall accuracy and F1-score of the two models on different dates when the threshold of probability was 0.5.

Index Type	Prediction Model	Date of the Prediction			
		February 18	March 6	April 23	May 9
OA	RVM	0.71	0.78	0.85	0.93
OA	Logistic	0.64	0.71	0.78	0.78
F1	RVM	0.70	0.79	0.86	0.92
F1	Logistic	0.64	0.74	0.75	0.79

Besides this, samples on Feb. 18, Mar. 6 (Dingyuan only), Apr. 23, and May 9 were randomly selected for 50 times, respectively, to get 50 curves on each date, then averaged to obtain the average ROC curve and calculate the AUC, as shown as Figure 9a–d. What stands out in the comparison is that the specificity of RVM was better, and the sensitivity of the Logistic model to diseased wheat had a slight advantage. The areas under the curves were all greater than 0.5, which indicated that the prediction of wheat FHB by both methods was better than a random guess and had a reference value. Besides this, the generalization ability and prediction ability of RVM were better than those of the Logistic model, to a lesser extent. When the date was closer to the onset period of FHB, the AUC also increased, and the prediction results were more accurate.

Moreover, to show the difference between the RVM constructed by multiple factors (remote sensing and weather features, Model 1) and that predicted by only one type of factor (remote sensing features on Apr. 23 or weather features, Model 2 or Model 3), we drew their average ROC curves in the same way (Figure 9e,f). Compared with Model 2, Model 1 greatly improved the prediction accuracy. As a classic FHB prediction model, the meteorological statistical model also had certain reference in

our experiments, partly because the weather features were calculated strictly according to the heading and flowering date of each pixel. However, when weather conditions suitable for FHB also occurred in areas with low severity, FHB infection could be inhibited when the host's own growth met certain conditions. In total, the integration of multiple factors is feasible and the remote sensing data can supplement the information of FHB. Therefore, in the period of disease development, the coupling growth stages, growth conditions, and weather conditions can improve the prediction accuracy of the severity of FHB and reveal its occurrence and development law.

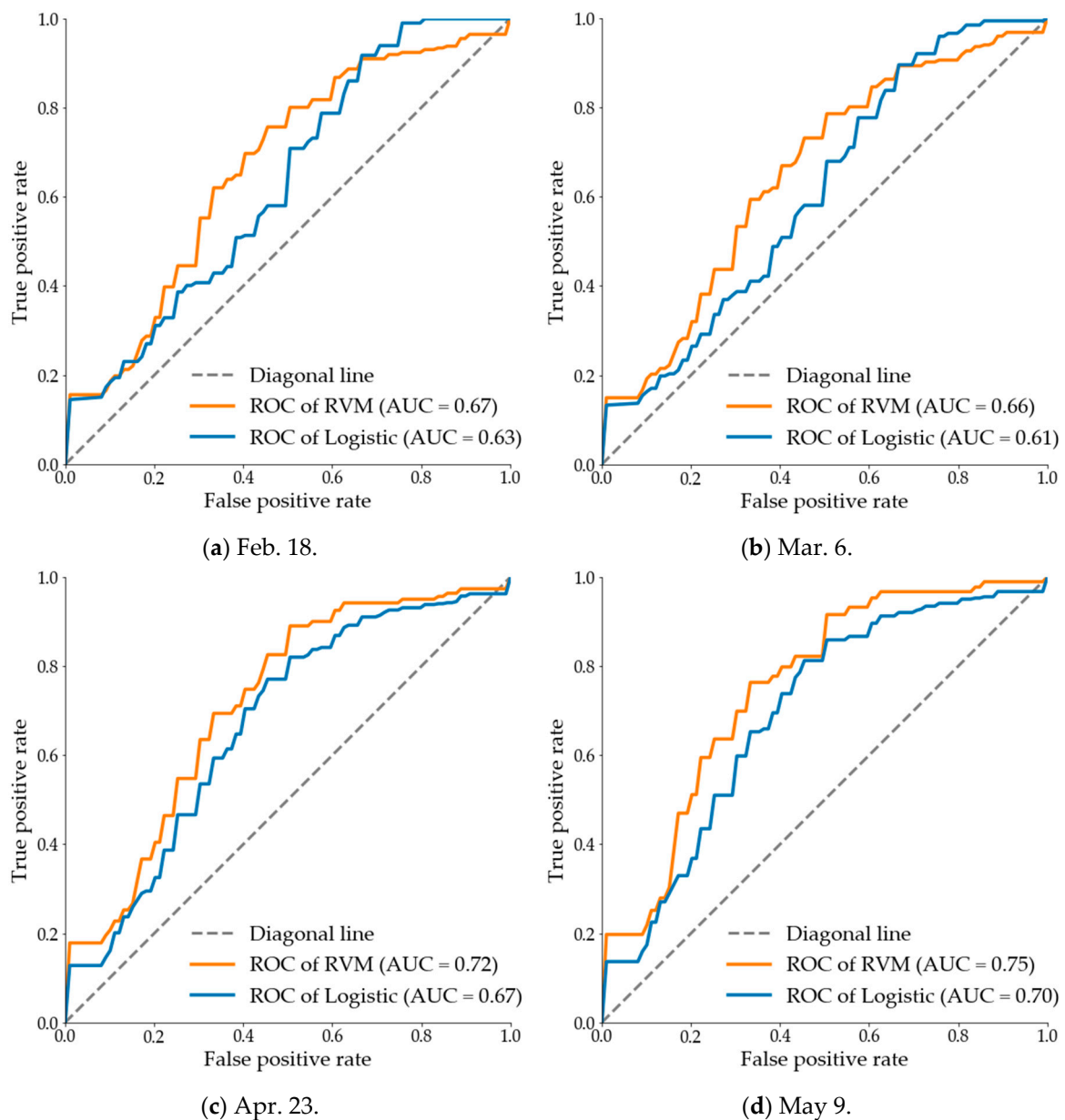


Figure 9. Cont.

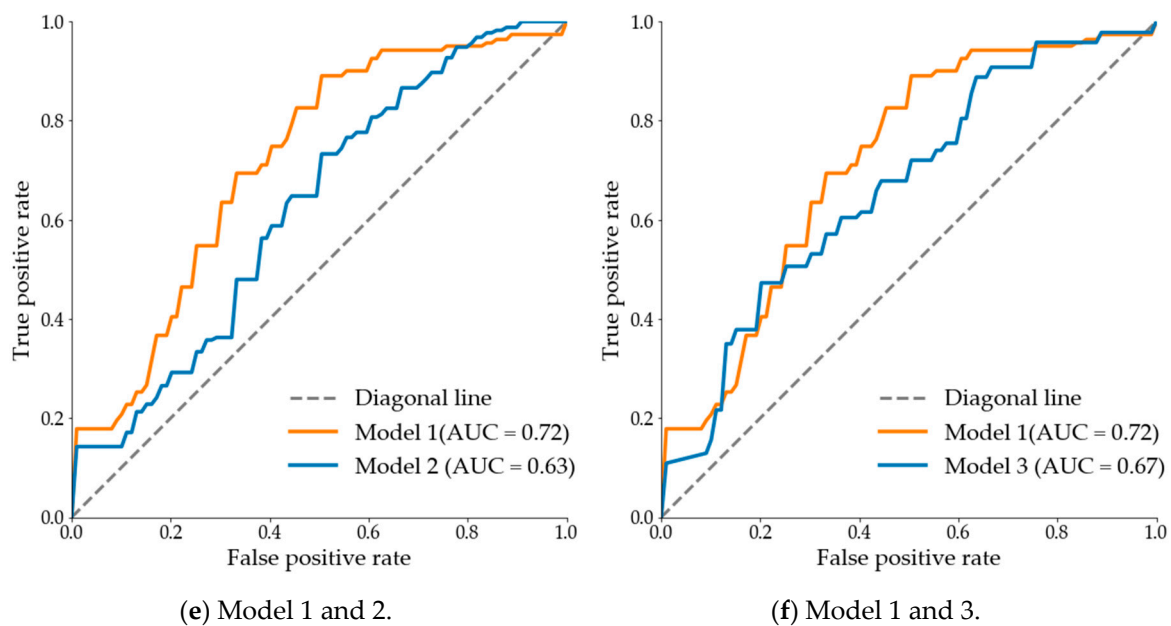


Figure 9. Average ROC curves and their corresponding AUC. (a–d) ROC curves of RVM and the Logistic model, using selected weather and remote sensing features from February 18, March 6, April 23, and May 9, respectively. (e,f) ROC curves of RVM, model 1, constructed by weather features and remote sensing features on April 23; model 2 constructed by only remote sensing features on April 23; model 3 constructed by only weather features.

4. Discussion

Researchers have developed various methods to predict this meteorological crop disease. The major merit of our method was the comprehensive consideration of host and habitat conditions [25], [20]. Besides, we realized dynamic prediction that made it possible for farmers to obtain early warning information. Time-series remote sensing data with high time resolution and the accumulated temperature were used to predict the heading and flowering dates of crops. Four indices, including PSRI, Red, Green, and NIR, were selected as remote sensing features to detect the growth of the crop. Besides this, five weather indices around heading or flowering were selected as weather features. The dynamic prediction was realized through inputting remote sensing features on different dates. Based on the nine optimized features, we compared the RVM with the Logistic model, and found that RVM was more suitable for wheat FHB prediction with a small sample of experimental data. When the date of remote sensing features was close to the stage of heading to flowering, the prediction accuracy was higher.

As the host of the pathogen, the growth stages and conditions of the crop play decisive roles. Every period could influence the FHB infection—for example, late seeding will result in a serious deficiency of wheat growth before winter, delay other growth periods, and shorten the grain filling period [48], which makes wheat more vulnerable to FHB [49]. However, heading and flowering are more critical to pathogen infection. Continuous rainy days in this time are likely to result in an epidemic of FHB [50]. MODIS data have been widely used in plant growth detection, especially in time-series applications [51,52]. Using long time-series MODIS data can accurately extract the green-up and heading dates of winter wheat [53–55], and the accumulated temperature data, as a significant factor indicating the transition of crop growth, can be used to predict growth stages [30]. The prediction of heading or flowering has more representational significance for the subsequent disease prediction, and reduced the uncertainty from the dormancy period. However, there is still something to be improved in our method. In our study area, the average area of wheat fields was 43.7 hectares in Changfeng and 48.4 hectares in Dingyuan. Though the growth periods in a small field were usually homogenous,

and the wheat fields in our study area were generally continuous, mixed pixels still influenced the extraction of growth stages. To obtain more convinced growth stage prediction results, we will try to collect some field data to explain the spatial distribution of the heading and flowering dates and use algorithms that deal with these mixed pixels. Besides, high spatial resolution remote sensing data provide detailed information on crop nutrition and structure. The increase in the PSRI can well reflect the stress of the crop canopy [11], and the other three parameters can offer information on crop growth. However, the Landsat-8 lack a red-edge band. The reflectance of 670–760 nm can be used to monitor plant activity, indicating the degree of crops under disease stress. Therefore, the spectral features will be improved in future work to illustrate the chlorophyll decomposition, early senescence, fast draining in spike water, and nitrogen concentration changes resulting from the invasion of the pathogen [56]. Weather conditions, especially temperature and humidity, are highly associated with epidemics. We found that weather indices near the predicted flowering stage were more critical to the development of FHB than those near the predicted heading date. Narrow periods around crop anthesis can be used to partly indicate FHB epidemics. This was consistent with the results of previous research [7,57].

Apart from these key factors that were considered in our methods, numerous other elements influence the occurrence of FHB infection, and the effect cannot be ignored under certain circumstances. First of all, there will be variances in the FHB resistance for different varieties of wheat, hence resulting in variances in their spectral features [2,56]. In the study area, farmers chose wheat varieties under the guidance of the local government, mainly Yangmai 25, Ningmai 9, Yangmai 15, etc. The characteristics of these varieties were similar, such as their high yield, but they were moderately susceptible to FHB. Though these wheat varieties have a similar susceptibility, a comparison between them is of great significance when the study area is larger. In our future work, we will try to find the differences in spectral features of these infected crops and realize the prediction in separate zones with different wheat varieties. Besides this, we will take the influence of mechanized operations into consideration—for example, stretcher sprays are 10% more effective than electric sprayers in FHB control [48]. The effect of fertilizers or other treatments is also important, especially nitrogen fertilization, which has been proved to be influential in FHB occurrence [2,58]. In our study area, there were no significant differences in these factors mentioned above, because the area was not large and the Chinese government has formulated a series of regulations to help farmers manage crops. However, to extend our methods to larger areas, we will try to collect this information and take full consideration in the future.

Our method was established to provide a more advantageous model for FHB severity prediction. In our numerical experiments, by integrating the remote sensing and weather features, RVM performed better when the remote sensing features were closer to the stage of heading to flowering, with the overall accuracy reaching 0.9 and the AUC around 0.7. The RVM and the Logistic model both proved to be useful in plant disease detection and prediction [13,36,59]. In our study, the accuracy and generalization ability of RVM on the four dates were higher than those of the Logistic model, and increased by about 10–20% and 6–9%, respectively. Moreover, when comparing the result of the RVM constructed by multiple factors and that constructed by only one type of factor, the comprehensive consideration of host and habitat conditions could improve the accuracy [60–62]. However, RVM performs well on small samples, but the universality of parameters of this kind of model is not that satisfying. That is, the parameters of the model will be different with the change in both time and space. A further study with deep learning algorithms could be considered to continuously refresh the parameters with new data input [20,63].

5. Conclusions

This study developed a dynamic prediction method for wheat FHB. Host and habitat conditions play decisive roles in FHB infection. The heading and flowering dates of winter wheat were predicted through long time-series MODIS LAI products. The remote sensing features on different dates and weather features around heading and flowering were combined to predict the severity of FHB.

The dynamic prediction was realized through inputting remote sensing features that change with time. With these crucial features as inputs, RVM performed well on the small sample of experimental data. The results showed that comprehensively considering those key factors can improve the prediction accuracy, and that when the date of remote sensing features was close to the stage of heading to flowering, the accuracy of the model was higher.

Some important issues should be taken into account in future work. Firstly, phenology information extraction should consider the influence of mixed pixels, and seeding dates can be used as explanatory factors. Besides this, combining the spectral bands that are sensitive to the changes resulting from FHB infection can improve the prediction accuracy. Other factors that influence the occurrence of FHB—for instance, the variety of wheat, mechanized operations, and fertilizers or other treatments—also play important roles. With the full consideration of these elements, adopting a model with a better generalization ability can make the method more suitable for larger areas.

Author Contributions: Conceptualization, Y.X., Y.D., and W.H.; Data curation, L.L. and H.M.; Formal analysis, Y.X.; Funding acquisition, Y.D. and W.H.; Investigation, Y.D., L.L., and H.M.; Methodology, Y.X. and Y.D.; Project administration, Y.D., W.H., H.Y., and K.W.; Resources, Y.D., L.L., and H.M.; Software, Y.X.; Supervision, Y.D., W.H., H.Y., and K.W.; Validation, Y.X.; Visualization, Y.X.; Writing—original draft, Y.X.; Writing—review and editing, Y.X., Y.D. and W.H. All authors have read and agreed to the published version of the manuscript.

Funding: This research was funded by the National Key R&D Program of China (2017YFE0122400), Beijing Nova Program of Science and Technology (Z191100001119089), Youth Innovation Promotion Association CAS (2017085), and the National Special Support Program for High-Level Personnel Recruitment (Ten-Thousand Talents Program) (Wenjiang Huang).

Conflicts of Interest: The authors declare no conflict of interest.

References

1. Singh, R.P.; Singh, P.K.; Rutkoski, J.; Hodson, D.P.; He, X.; Jørgensen, L.N.; Hovmøller, M.S.; Huerta-Espino, J. Disease Impact on Wheat Yield Potential and Prospects of Genetic Control. *Annu. Rev. Phytopathol.* **2016**, *54*, 303–322. [[CrossRef](#)]
2. Dweba, C.C.; Figlan, S.; Shimelis, H.A.; Motaung, T.E.; Sydenham, S.; Mwadzingeni, L.; Tsilo, T.J. Fusarium head blight of wheat: Pathogenesis and control strategies. *Crop Prot.* **2017**, *91*, 114–122. [[CrossRef](#)]
3. Salgado, J.D.; Madden, L.V.; Paul, P.A. Quantifying the effects of Fusarium head blight on grain yield and test weight in soft red winter wheat. *Phytopathology* **2015**, *105*, 295–306. [[CrossRef](#)]
4. Palazzini, J.; Roncallo, P.; Cantoro, R.; Chiotta, M.; Yerkovich, N.; Palacios, S.; Echenique, V.; Torres, A.; Ramirez, M.; Karlovsky, P.; et al. Biocontrol of Fusarium graminearum sensu stricto, Reduction of Deoxynivalenol Accumulation and Phytohormone Induction by Two Selected Antagonists. *Toxins* **2018**, *10*, 88. [[CrossRef](#)]
5. Cowger, C.; Smith, J.; Boos, D.; Bradley, C.A.; Ransom, J.; Bergstrom, G.C. Managing a Destructive, Episodic Crop Disease: A National Survey of Wheat and Barley Growers' Experience With Fusarium Head Blight. *Plant Dis.* **2020**, *104*, 634–648. [[CrossRef](#)]
6. Steiner, B.; Buerstmayr, M.; Michel, S.; Schweiger, W.; Lemmens, M.; Buerstmayr, H. Breeding strategies and advances in line selection for Fusarium head blight resistance in wheat. *Trop. Plant Pathol.* **2017**, *42*, 165–174. [[CrossRef](#)]
7. Shah, D.A.; De Wolf, E.D.; Paul, P.A.; Madden, L.V. Functional data analysis of weather variables linked to Fusarium head blight epidemics in the United States. *Phytopathology* **2019**, *109*, 96–110. [[CrossRef](#)]
8. Birr, T.; Verreet, J.A.; Klink, H. Prediction of deoxynivalenol and zearalenone in winter wheat grain in a maize-free crop rotation based on cultivar susceptibility and meteorological factors. *J. Plant Dis. Prot.* **2019**, *126*, 13–27. [[CrossRef](#)]
9. El Jarroudi, M.; Lahlali, R.; Kouadio, L.; Denis, A.; Belleflamme, A.; El Jarroudi, M.; Boulif, M.; Mahyou, H.; Tychon, B. Weather-based predictive modeling of wheat stripe rust infection in Morocco. *Agronomy* **2020**, *10*, 280. [[CrossRef](#)]
10. Merle, I.; Tixier, P.; Virginio Filho, E.d.M.; Cilas, C.; Avelino, J. Forecast models of coffee leaf rust symptoms and signs based on identified microclimatic combinations in coffee-based agroforestry systems in Costa Rica. *Crop Prot.* **2020**, *130*, 105046. [[CrossRef](#)]

11. Yudarwati, R.; Hongo, C.; Sigit, G.; Barus, B.; Utoyo, B. Bacterial Leaf Blight Detection in Rice Crops Using Ground-Based Spectroradiometer Data and Multi-temporal Satellites Images. *J. Agric. Sci.* **2020**, *12*, 38. [[CrossRef](#)]
12. Zhang, J.; Yuan, L.; Nie, C.; Wei, L.; Yang, G. Forecasting of powdery mildew disease with multi-sources of remote sensing information. In Proceedings of the Third International Conference on Agro-Geoinformatics, Beijing, China, 11–14 August 2014; pp. 1–5.
13. Ma, H.; Huang, W.; Jing, Y. Wheat powdery mildew forecasting in filling stage based on remote sensing and meteorological data. *Trans. Chin. Soc. Agric. Eng.* **2016**, *32*, 165–172. [[CrossRef](#)]
14. Ma, H.; Huang, W.; Jing, Y.; Yang, C.; Han, L.; Dong, Y.; Ye, H.; Shi, Y.; Zheng, Q.; Liu, L.; et al. Integrating Growth and Environmental Parameters to Discriminate Powdery Mildew and Aphid of Winter Wheat Using Bi-Temporal Landsat-8 Imagery. *Remote Sens.* **2019**, *11*, 846. [[CrossRef](#)]
15. Zheng, Q.; Huang, W.; Cui, X.; Dong, Y.; Shi, Y.; Ma, H.; Liu, L. Identification of Wheat Yellow Rust Using Optimal Three-Band Spectral Indices in Different Growth Stages. *Sensors* **2018**, *19*, 35. [[CrossRef](#)]
16. Loladze, A.; Rodrigues, F.A.; Toledo, F.; Vicente, F.S.; Gérard, B.; Boddupalli, M.P. Application of remote sensing for phenotyping tar spot complex resistance in maize. *Front. Plant Sci.* **2019**, *10*, 1–10. [[CrossRef](#)]
17. Anees, A.; Aryal, J. Near-real time detection of beetle infestation in pine forests using MODIS data. *IEEE J. Sel. Top. Appl. Earth Obs. Remote Sens.* **2014**, *7*, 3713–3723. [[CrossRef](#)]
18. Li, W.; Huang, W.; Dong, Y.; Chen, H.; Wang, J.; Shan, J. Estimation on winter wheat scab based on combination of temperature, humidity and remote sensing vegetation index. *Trans. Chin. Soc. Agric. Eng.* **2017**, *33*, 203–210. [[CrossRef](#)]
19. Mahlein, A. Plant Disease Detection by Imaging Sensors—Parallels and Specific Demands for Precision Agriculture and Plant Phenotyping. *Plant Dis.* **2016**, *100*, 241–251. [[CrossRef](#)]
20. Zhang, J.; Huang, Y.; Pu, R.; Gonzalez-Moreno, P.; Yuan, L.; Wu, K.; Huang, W. Monitoring plant diseases and pests through remote sensing technology: A review. *Comput. Electron. Agric.* **2019**, *165*, 104943. [[CrossRef](#)]
21. Luo, J.; Zhao, C.; Huang, W.; Zhang, J.; Zhao, J.; Dong, Y.; Yuan, L.; Du, S. Discriminating Wheat Aphid Damage Degree Using 2-Dimensional Feature Space Derived from Landsat 5 TM. *Sens. Lett.* **2012**, *10*, 608–614. [[CrossRef](#)]
22. Shi, Y.; Huang, W.; González-Moreno, P.; Luke, B.; Dong, Y.; Zheng, Q.; Ma, H.; Liu, L. Wavelet-Based Rust Spectral Feature Set (WRSFs): A Novel Spectral Feature Set Based on Continuous Wavelet Transformation for Tracking Progressive Host–Pathogen Interaction of Yellow Rust on Wheat. *Remote Sens.* **2018**, *10*, 525. [[CrossRef](#)]
23. Ampatzidis, Y.; Partel, V. UAV-Based High Throughput Phenotyping in Citrus Utilizing Multispectral Imaging and Artificial Intelligence. *Remote Sens.* **2019**, *11*, 410. [[CrossRef](#)]
24. Anees, A.; Aryal, J. A statistical framework for near-real time detection of beetle infestation in pine forests using MODIS data. *IEEE Geosci. Remote Sens. Lett.* **2014**, *11*, 1717–1721. [[CrossRef](#)]
25. Liu, L.; Dong, Y.; Huang, W.; Du, X.; Ren, B.; Huang, L.; Zheng, Q.; Ma, H. A Disease Index for Efficiently Detecting Wheat Fusarium Head Blight Using Sentinel-2 Multispectral Imagery. *IEEE Access* **2020**, *8*, 52181–52191. [[CrossRef](#)]
26. Chen, Y.; Wang, J.; Yang, R.; Ma, Z. Current situation and management strategies of Fusarium head blight in China. *Plant Prot.* **2017**, *43*, 11–17.
27. Xu, J.; Chen, L.; Ding, K.J. Resistance Analysis of Wheat Varieties to Scab in Anhui Province. *J. Anhui Agric. Sci.* **2019**, *47*, 172–173.
28. Rokni, K.; Musa, T.A. Normalized difference vegetation change index: A technique for detecting vegetation changes using Landsat imagery. *CATENA* **2019**, *178*, 59–63. [[CrossRef](#)]
29. Huang, W.; Guan, Q.; Luo, J.; Zhang, J.; Zhao, J.; Liang, D.; Huang, L.; Zhang, D. New Optimized Spectral Indices for Identifying and Monitoring Winter Wheat Diseases. *IEEE J. Sel. Top. Appl. Earth Obs. Remote Sens.* **2014**, *7*, 2516–2524. [[CrossRef](#)]
30. Huang, J.; Zhao, J.; Wang, X.; Xie, Z.; Zhuo, W.; Huang, R. Extraction Method of Growth Stages of Winter Wheat Based on Accumulated Temperature and Remote Sensing Data. *Nongye Jixie Xuebao/Trans. Chin. Soc. Agric. Mach.* **2019**, *50*, 169–176. [[CrossRef](#)]
31. Zhou, J.; Mao, S.; Wang, J.; Meng, F.; Ye, C.; Li, C. Temperature Evolution and Indicator of Wheat Growth Period in Beijing. *Crops.* **2016**, *3*, 116–122.

32. Eilers, P.H.C.; Pesendorfer, V.; Bonifacio, R. Automatic smoothing of remote sensing data. In Proceedings of the 2017 9th International Workshop on the Analysis of Multitemporal Remote Sensing Images (MultiTemp), Brugge, Belgium, 27–29 June 2017; pp. 1–3.
33. Kong, D.; Zhang, Y.; Gu, X.; Wang, D. A robust method for reconstructing global MODIS EVI time series on the Google Earth Engine. *ISPRS J. Photogramm. Remote Sens.* **2019**, *155*, 13–24. [[CrossRef](#)]
34. Hou, X.; Gao, S.; Niu, Z.; Xu, Z. Extracting grassland vegetation phenology in North China based on cumulative SPOT-VEGETATION NDVI data. *Int. J. Remote Sens.* **2014**, *35*, 3316–3330. [[CrossRef](#)]
35. Hou, X.; Sui, X.; Liang, S.; Wang, M.; Dong, M. Comparison of Five Methods for Phenology Extraction of Winter Wheat. *Remote Sens. Inf.* **2017**, *32*, 65–70.
36. Shah, D.A.; Molineros, J.E.; Paul, P.A.; Willyerd, K.T.; Madden, L.V.; De Wolf, E.D. Predicting fusarium head blight epidemics with weather-driven pre- and post-anthesis logistic regression models. *Phytopathology* **2013**, *103*, 906–919. [[CrossRef](#)]
37. Ferrigo, D.; Raiola, A.; Causin, R. Fusarium Toxins in Cereals: Occurrence, Legislation, Factors Promoting the Appearance and Their Management. *Molecules* **2016**, *21*, 627. [[CrossRef](#)]
38. Gilbert, J.; Haber, S. Overview of some recent research developments in fusarium head blight of wheat. *Can. J. Plant Pathol.* **2013**, *35*, 149–174. [[CrossRef](#)]
39. Cowger, C.; Weisz, R.; Arellano, C.; Murphy, P. Profitability of integrated management of fusarium head blight in North Carolina winter wheat. *Phytopathology* **2016**, *106*, 814–823. [[CrossRef](#)]
40. Tipping, M.E. Sparse Bayesian Learning and the Relevance Vector Machine. *J. Mach. Learn. Res.* **2001**, *1*, 211–244. [[CrossRef](#)]
41. Liu, J.; Zhou, X.; Huang, J.; Liu, S.; Li, H.; Wen, S.; Liu, J. Semantic classification for hyperspectral image by integrating distance measurement and relevance vector machine. *Multimed. Syst.* **2017**, *23*, 95–104. [[CrossRef](#)]
42. Graves, S.; Asner, G.; Martin, R.; Anderson, C.; Colgan, M.; Kalantari, L.; Bohlman, S. Tree Species Abundance Predictions in a Tropical Agricultural Landscape with a Supervised Classification Model and Imbalanced Data. *Remote Sens.* **2016**, *8*, 161. [[CrossRef](#)]
43. Guo, A.; Huang, W.; Ye, H.; Dong, Y.; Ma, H.; Ren, Y. Identification of Wheat Yellow Rust using Spectral and Texture Features of Hyperspectral Images. *Remote Sens.* **2020**, *12*, 1419. [[CrossRef](#)]
44. Immitzer, M.; Vuolo, F.; Atzberger, C. First Experience with Sentinel-2 Data for Crop and Tree Species Classifications in Central Europe. *Remote Sens.* **2016**, *8*, 166. [[CrossRef](#)]
45. Sokolova, M.; Lapalme, G. A systematic analysis of performance measures for classification tasks. *Inf. Process. Manag.* **2009**, *45*, 427–437. [[CrossRef](#)]
46. Kumar, R.; Indrayan, A. Receiver Operating Characteristic (ROC) Curve for Medical Researchers. *INDIAN Pediatr.* **2011**, *48*, 277–287. [[CrossRef](#)]
47. Jin, X.; Jie, L.; Wang, S.; Qi, H.; Li, S. Classifying Wheat Hyperspectral Pixels of Healthy Heads and Fusarium Head Blight Disease Using a Deep Neural Network in the Wild Field. *Remote Sens.* **2018**, *10*, 395. [[CrossRef](#)]
48. Yongming, C.; Fugen, L.; Yang, Z.; Tingting, H.; Lei, D.; Aizhong, M.; Xiaosong, C.; Reasons, T.P. The Population Reasons and Control Measures of Wheat Scab in the East of Jiangsu. *J. Agric.* **2015**, *5*, 33–38.
49. Gorczyca, A.; Oleksy, A.; Gala-Czekaj, D.; Urbaniak, M.; Laskowska, M.; Waškiewicz, A.; Stępień, Ł. Fusarium head blight incidence and mycotoxin accumulation in three durum wheat cultivars in relation to sowing date and density. *Sci. Nat.* **2018**, *105*, 2. [[CrossRef](#)]
50. Wegulo, S.N.; Baenziger, P.S.; Hernandez Nopsa, J.; Bockus, W.W.; Hallen-Adams, H. Management of Fusarium head blight of wheat and barley. *Crop Prot.* **2015**, *73*, 100–107. [[CrossRef](#)]
51. Lopresti, M.F.; Di Bella, C.M.; Degioanni, A.J. Relationship between MODIS-NDVI data and wheat yield: A case study in Northern Buenos Aires province, Argentina. *Inf. Process. Agric.* **2015**, *2*, 73–84. [[CrossRef](#)]
52. Sakamoto, T.; Gitelson, A.A.; Arkebauer, T.J. MODIS-based corn grain yield estimation model incorporating crop phenology information. *Remote Sens. Environ.* **2013**, *131*, 215–231. [[CrossRef](#)]
53. Zhou, H.; Wang, N.; Huang, Y.; Wang, J.; Zhang, L. Comparison and Analysis of Remotely Sensed Time Series of Reconstruction Models at Various Intervals. *J. Geo-Inf. Sci.* **2016**, *18*, 1410–1417.
54. Cai, Z.; Jönsson, P.; Jin, H.; Eklundh, L. Performance of smoothing methods for reconstructing NDVI time-series and estimating vegetation phenology from MODIS data. *Remote Sens.* **2017**, *9*, 1271. [[CrossRef](#)]

55. Jamali, S.; Jönsson, P.; Eklundh, L.; Ardö, J.; Seaquist, J. Detecting changes in vegetation trends using time series segmentation. *Remote Sens. Environ.* **2015**, *156*, 182–195. [[CrossRef](#)]
56. Alisaac, E.; Behmann, J.; Kuska, M.T.; Dehne, H.W.; Mahlein, A.K. Hyperspectral quantification of wheat resistance to Fusarium head blight: Comparison of two Fusarium species. *Eur. J. Plant Pathol.* **2018**, *152*, 869–884. [[CrossRef](#)]
57. Shah, D.A.; De Wolf, E.D.; Paul, P.A.; Madden, L.V. Predicting fusarium head blight epidemics with boosted regression trees. *Phytopathology* **2014**, *104*, 702–714. [[CrossRef](#)]
58. Hofer, K.; Bartheimer, G.; Schmidhalter, U.; Habler, K.; Rychlik, M.; Hüchelhoven, R.; Hess, M. Effect of nitrogen fertilization on Fusarium head blight in spring barley. *Crop Prot.* **2016**, *88*, 18–27. [[CrossRef](#)]
59. Rana, A.; Mittal, A. Herbal Plant Classification and Leaf Disease Identification Using MPEG-7 Feature Descriptor and Logistic Regression. *Adv. Intell. Syst. Comput.* **2020**, *1048*, 761–772. [[CrossRef](#)]
60. Ma, H.; Jing, Y.; Huang, W.; Shi, Y.; Dong, Y.; Zhang, J.; Liu, L. Integrating Early Growth Information to Monitor Winter Wheat Powdery Mildew Using Multi-Temporal Landsat-8 Imagery. *Sensors* **2018**, *18*, 3290. [[CrossRef](#)]
61. Li, W.; Liu, Y.; Chen, H.; Zhang, C.C. Estimation model of winter wheat disease based on meteorological factors and spectral information. *Food Prod. Process. Nutr.* **2020**, *2*, 1–7. [[CrossRef](#)]
62. Huang, S.; Miao, Y.; Yuan, F.; Gnyp, M.; Yao, Y.; Cao, Q.; Wang, H.; Lenz-Wiedemann, V.; Bareth, G. Potential of RapidEye and WorldView-2 Satellite Data for Improving Rice Nitrogen Status Monitoring at Different Growth Stages. *Remote Sens.* **2017**, *9*, 227. [[CrossRef](#)]
63. Golhani, K.; Balasundram, S.K.; Vadmalai, G.; Pradhan, B. A review of neural networks in plant disease detection using hyperspectral data Airborne Imaging Spectrometer for Applications. *Inf. Process. Agric.* **2018**, *5*, 354–371. [[CrossRef](#)]



© 2020 by the authors. Licensee MDPI, Basel, Switzerland. This article is an open access article distributed under the terms and conditions of the Creative Commons Attribution (CC BY) license (<http://creativecommons.org/licenses/by/4.0/>).